Communications on Applied Nonlinear Analysis
ISSN: 1074-133X
Vol 31 No. 2 (2024)

Flow of Hybrid Dust Micropolar Nanofluids Along the Symmetric Riga Surface with Heat Generation and Application of Cattaneo-Christov Theory

[1] Dr. E. Rama, [2] M Annapoorna

[1]Associate Professor, Department of Mathematics, Osmania University, Hyderabad, India

[2]Degree Lecturer, Department of Mathematics, TSWRDCW, Telangana, India

Article History:

Received: *01-02-2024*

Revised: *15-04-2024*

Accepted: *30-04-2024*

Abstract: This study investigates the mechanical characteristics of a hybrid nanofluid containing dust and micropolar particles, flowing under mixed convection past a symmetric Riga surface using the Cattaneo-Christov (C-C) heat flux theory with consideration for heat generation effects. The analysis focuses on dust micropolar flow within a porous medium with a combination of hybrid nanoparticles CNTs - Fe_3O_4 with blood. The mathematical model describing this system involves a set of partial differential equations (PDEs), which are transformed into dimensionless ordinary differential equations (ODEs) and eventually into a form that can be solved using the MATLAB program. Graphical representations are employed to examine and discuss the impact of various flow parameters on the velocity and temperature profiles of the dust micropolar hybrid nanofluid. Several key findings emerge from this investigation. It is anticipated that an increase in the interaction between fluid particle parameters will result in a decrease in the temperature of the fluid phase and an increase in the temperature of the dust phase. Moreover, the study reveals that the Nusselt number is influenced by the mixed convection effects. Additionally, larger values of the heat generation parameter lead to higher temperatures in both the fluid phase and the dust phase.

Conclusion: In summary, this study comprehensively investigates the dynamics of nanofluid flows over a Riga surface, considering parameters like R_d, Pr, and βv. The findings highlight their significant impact on temperature distribution, fluid flow patterns, and friction forces. The results offer insights crucial for optimizing engineering systems like cooling technologies and heat exchangers. This research advances our understanding of nanofluid dynamics and provides valuable guidance for future studies and practical applications.

Keywords: Micropolar Dust phase, Porous medium, a symmetric Riga Surface, Cattaneo-Christov Theory, Heat generation, Thermal radiation.

1. Abstract

This study investigates the mechanical characteristics of a hybrid nanofluid containing dust and micropolar particles, flowing under mixed convection past a symmetric Riga surface using the Cattaneo-Christov (C-C) heat flux theory with consideration for heat generation effects. The analysis focuses on dust micropolar flow within a porous medium with a

combination of hybrid nanoparticles CNTs - Fe_3O_4 with blood. The mathematical model describing this system involves a set of partial differential equations (PDEs), which are transformed into dimensionless ordinary differential equations (ODEs) and eventually into a form that can be solved using the MATLAB program. Graphical representations are employed to examine and discuss the impact of various flow parameters on the velocity and temperature profiles of the dust micropolar hybrid nanofluid. Several key findings emerge from this investigation. It is anticipated that an increase in the interaction between fluid particle parameters will result in a decrease in the temperature of the fluid phase and an increase in the temperature of the dust phase. Moreover, the study reveals that the Nusselt number is influenced by the mixed convection effects. Additionally, larger values of the heat generation parameter lead to higher temperatures in both the fluid phase and the dust phase.

2. Introduction

Recently, nanotechnology has been widely used in therapeutic methods such as the use of polymeric nanoparticles, silica nanoparticles, gold nanomaterials, magnetic nanoparticles, and nanotubes (CNTs). Graphite tubes with diameters commonly measured in nano-meters are known as (CNTs). There are two kinds of carbon nanotubes: first kind Multi-wall carbon nanotubes (MWCNTs) have more than one grapheme layer and are seamless cylinders of carbon allotropes with a diameter of 5.0–20 nm., which were discovered by researchers Radushkevich and Lukyanovich [1]. Iijima's seminal work on helical microtubules of graphitic carbon in 1991 expanded the understanding of carbon nanostructures, setting the stage for their diverse applications [2]. Since then, research has extensively explored the synthesis, properties, and applications of CNTs, including their use in nanofluids to improve thermal conductivity, as demonstrated by Murshd et al. [3] and Choi et al. [7]. Moreover, the development of hybrid nanofluids, combining different nanoparticles to achieve synergistic effects, has opened new avenues for enhancing heat transfer properties. Studies by Rahman et al. [14] and Khan et al. [23] have investigated the thermal characteristics of hybrid nanofluids, revealing their potential for various applications. Additionally, the incorporation of magnetic nanoparticles, such as Fe3O4, in nanofluids has enabled precise control over fluid flow and heat transfer, as demonstrated by Manaa et al. [17] and Mehryan et al. [18].

In parallel, advancements in fluid dynamics have led to the exploration of complex flow phenomena over surfaces with specific geometries, such as the Riga surface. This surface, introduced by Gailitis in 1961 [37], offers unique flow characteristics that influence heat transfer processes. Recent studies by Abbas et al. [41] and Islam et al. [43] have investigated the flow of micropolar fluids over Riga surfaces, shedding light on the underlying mechanisms governing these flows.

The primary objective of this study is to investigate two-dimensional, incompressible dust micropolar flow within a porous medium, focusing on the flow over a symmetric Riga plate. Blood serves as the base liquid, with hybrid nanoparticles consisting of carbon nanotubes (CNTs) and Fe3O4 incorporated into the fluid. The analysis considers various factors, including heat generation, thermal radiation, and mixed convection effects. Notably, the Cattaneo-Christov (C-C) heat flux theory is employed to formulate the energy and mass

equations governing the flow. Through the use of tables, charts, and figures, the study explores the influence of key parameters on velocity, temperature, hybrid nanofluid concentration, local skin friction, and local Nusselt number, providing insights into the complex interactions within the system.

3. Objectives

This paper aims to address several objectives. Firstly, it investigates the behavior of two-dimensional, incompressible dust micropolar flow adjacent to a symmetric Riga plate. Secondly, it explores the implications of using blood as the base liquid and incorporating hybrid nanoparticles, specifically carbon nanotubes (CNTs) and Fe3O4, into the fluid medium. Thirdly, the study delves into the effects of various factors such as heat generation, thermal radiation, and mixed convection on the flow dynamics. Additionally, the paper employs the Cattaneo-Christov (C-C) heat flux theory to formulate energy and mass equations governing the flow, offering insights into the thermal characteristics of the system. Lastly, through the utilization of tables, charts, and figures, the research aims to elucidate the influence of key parameters like velocity, temperature, hybrid nanofluid concentration, local skin friction, and local Nusselt number, facilitating a comprehensive understanding of the flow behavior and its underlying mechanisms.

4. Problem Formulation

Consider the problem of two-phase, 2D steady laminar flow and heat transfer in a micropolar dusty fluid embedded in a porous vertical Riga surface. Figure 2 shows a theoretical and numerical examination of shaped hybrid nanofluid flow with attendance of linear thermal radiation and heat generation effects using the C-C heat flux model.

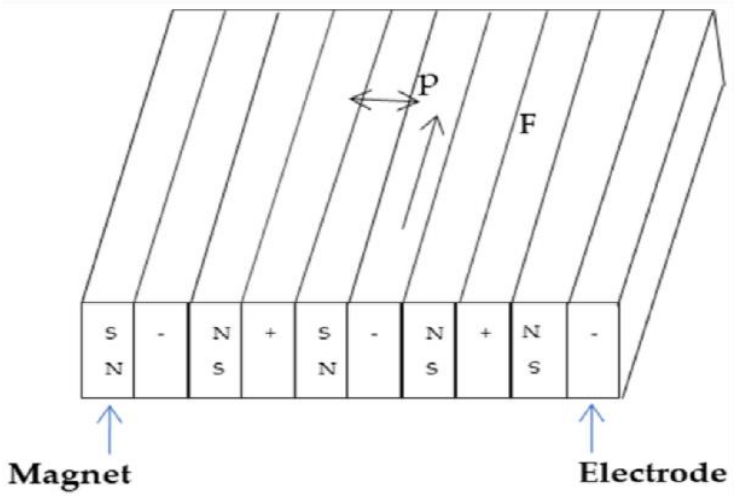

Figure 1: Riga plate geometry.

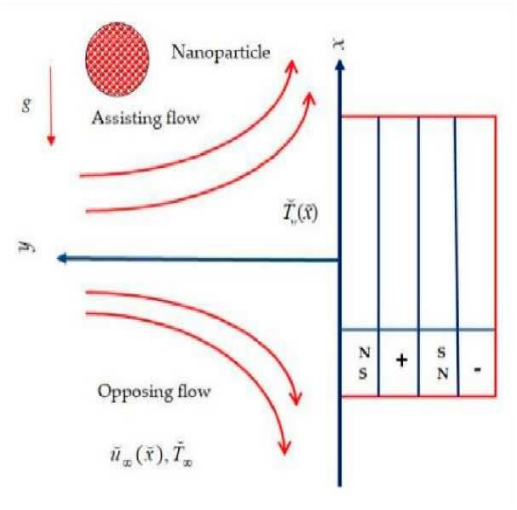

Figure 2: Flow configuration and coordinate system.

We have considered velocity and temperature in The x-y coordinate system in Cartesian coordinates, are the denote velocity is u_∞= cx and temperature is T_w(x)=T_∞+bx with T_w(x) > T_∞ , respectively, In this context, the coordinate system considers the direction of x along the Riga's surface, while y represents the direction normal to it., T_∞,b and c represent the ambient temperature and positive constants, respectively.

The vector representations of the governing equations for a motion micropolar flow and dust flow with spherical properties are as follows:

4.1 Micropolar fluid

$$\nabla.\mathrm{V} = 0, \tag{1}$$

$$\rho_{hnf}(\mathrm{V}.\nabla)\mathrm{V} = \left(\mu_{hnf} + \mathrm{k}\right)\nabla^2\mathrm{V} + \mathrm{k}(\nabla \times N) + k^* s\left(u_p - \mathrm{u}\right) - \frac{\mu_{hnf}}{K_p}u + g\beta_{hnf}(T - T_\infty) + f, \tag{2}$$

$$j\rho_{hnf}(\mathrm{V}.\nabla)N = \mathrm{j}\left(\mu_{hnf} + \frac{\mathrm{k}}{2}\right)\nabla^2\mathrm{N} + k(\nabla \times \mathrm{V}) - 2\mathrm{kN}, \tag{3}$$

$$(\rho c_p)_{hnf}(\mathrm{V}.\nabla)T + \nabla q^r - [Q_0(T - T_\infty) + \frac{\rho_p(c_p)_f}{\tau_T}\left(T_p - \mathrm{T}\right) + \frac{\rho_p}{\tau_v}\left(u_p - \mathrm{u}\right)^2] = -\nabla.\check{\mathrm{q}}. \tag{4}$$

Where $\check{\mathrm{q}}$ is heat flux. The Cattaneo-Christov expression (C-C) for heat flux is given as

$$\check{\mathrm{q}} + \gamma_t(\mathrm{V}.\nabla\check{\mathrm{q}} - \check{\mathrm{q}}.\nabla\mathrm{V}) = -k_{hnf}\nabla\mathrm{T}$$

where γ_t represents thermal relaxation time, V signifies velocity, f the Lorentz force.

4.2 Dust fluid

$$\nabla.\mathrm{V}_p = 0, \tag{5}$$

$$\rho_p\left(\mathrm{V}_p.\nabla\right)\mathrm{V}_p = -k^* s\left(u_p - \mathrm{u}\right), \tag{6}$$

$\tau_T c_m(\mathrm{V}_p.\nabla)T_p = -(c_p)_f(T_p - \mathrm{T}).$

(7)

The governing equations for both the fluid and dust phases are developed using the assumptions stated above [25-28].

4.3 Fluid flow and heat transfer in micropolar systems

$$\partial_x u + \partial_y v = 0 \tag{8}$$

$$u\partial_x u + v\partial_y u = \left(\frac{\mu_{hnf}+\mathrm{k}}{\rho_{hnf}}\right)\partial_{yy}\mathrm{u} + \frac{k^* s}{\rho_{hnf}}(u_p - \mathrm{u}) + \frac{\mathrm{k}}{\rho_{hnf}}\partial_y N - \frac{\mu_{hnf}}{\rho_{hnf}K_p}u + \frac{\pi j_0 M_0}{8\rho_{hnf}}e^{\left(-\frac{\pi}{a}y\right)} + g\beta_{hnf}(T - T_\infty) \tag{9}$$

$$u\partial_x N + v\partial_y N = \left(\frac{\mu_{hnf}+\frac{\mathrm{k}}{2}}{\rho_{hnf}}\right)\partial_{yy}\mathrm{N} - \frac{k}{j\rho_{hnf}}(2\mathrm{N} + \partial_y u) \tag{10}$$

$$u\partial_x T + v\partial_y T + \gamma_t\left(2uv\partial_{xy}T + u^2\partial_{xx}T + v^2\partial_{yy}T + (u\partial_x u + v\partial_y u)\partial_x T + (u\partial_x v + v\partial_y v)\partial_y T - \frac{Q_0}{(\rho c_p)_{hnf}}(u\partial_x T + v\partial_y T)\right) = \frac{k_{hnf}}{(\rho c_p)_{hnf}}\partial_{yy}T - \partial_y q^r + \frac{\rho_p(c_p)_f}{\tau_T(\rho c_p)_{hnf}}(T_p - T) + \frac{\rho_p}{\tau_v(\rho c_p)_{hnf}}(u_p - u)^2 + \frac{Q_0}{(\rho c_p)_{hnf}}(T - T_\infty) \tag{11}$$

4.4 Heat transfer and dust particle flow

$$\partial_x u_p + \partial_y v_p = 0 \tag{12}$$

$$u_p\partial_x u_p + v_p\partial_y u_p = \frac{k^* s}{\rho_p}(\mathrm{u} - u_p) \tag{13}$$

$$u_p\partial_x T_p + v_p\partial_y T_p = -\frac{(c_p)_f}{\tau_T c_m}(T_p - T) \tag{14}$$

The corresponding boundary conditions for given problem is

$$u = u_\mathrm{w} = \mathrm{cx}\ , \mathrm{v} = 0\ ,\ \ T = T_w(x) = T_\infty + bx,\ \ N = -n\partial_y u \quad at\ y = 0 \tag{15}$$

$$u \to 0\ , u_p \to 0\ , v_p \to \mathrm{v}, T \to T_\infty\ \ , T_p \to T_\infty\ ,\ N \to 0 \qquad as\ y \to \infty \tag{16}$$

Here (u, v) and (u_p, v_p) these denote the velocity components along the x and y axes, respectively , ρ_{hnf} , $(\rho c_p)_{hnf}$, $\mu_{hnf}, k_{\mathrm{hnf}}$ and σ_{hnf} represent the density, volumetric heat capacity, viscosity, and thermal conductivity of the hybrid nanofluid, respectively. K_p permeability of porous medium , $k^* = 6\pi c\mu_f$ is the Stokes drag constant, S is the density of the dust particles, the length is $j = \frac{\nu_{hnf}}{c}$ and $K = \frac{k}{\mu_f}$ is the parameter of material T, the velocity of angular is N, τ_v and τ_T are the particle phase relaxation and energy equilibrium times, and Q_0 is the heat generation. The term q^r is refers to the Rosseland radiative heat flux, which is defined as $q^r = -\frac{4\sigma^*}{3k^{**}}\partial_y T^4 = -\frac{16\sigma^*}{3k^{**}}T_\infty^3\partial_y T$. Table 1 Utilized models for the thermophysical properties of the hybrid nanofluid [6,10].

Properties	**Hybrid-nanofluid**	**Nanofluid**
Dynamic viscosity	$\mu_{\mathrm{hnf}} = \mu_{\mathrm{bf}}(1-\varphi_2)^{-2.5}$	$\mu_{\mathrm{bf}} = \mu_{\mathrm{f}}(1-\varphi_1)^{-2.5}$
Density	$\rho_{\mathrm{hnf}} = (1-\varphi_2)\rho_{\mathrm{bf}} + \varphi_2\rho_2,$	$\rho_{\mathrm{bf}} = (1-\varphi_1)\rho_{\mathrm{f}} + \varphi_1\rho_1$
Heat capacity	$(\rho c_p)_{\mathrm{hnf}} = (1-\varphi_2)(\rho c_p)_{\mathrm{bf}} + \varphi_2(\rho c_p)_2,$	$(\rho c_p)_{\mathrm{bf}} = (1-\varphi_1)(\rho c_p)_{\mathrm{f}} + \varphi_1(\rho c_p)_1$
Thermal conduc.	$\frac{k_{\mathrm{hnf}}}{k_{\mathrm{bf}}} = \frac{(k_2+(\hat{m}-1)k_{\mathrm{bf}})-(\hat{m}-1)\varphi_2(k_{\mathrm{bf}}-k_2)}{(k_2+(\hat{m}-1)k_{\mathrm{bf}})+\varphi_2(k_{\mathrm{bf}}-k_2)},$	$\frac{k_{\mathrm{bf}}}{k_{\mathrm{f}}} = \frac{(k_1+(\hat{m}-1)k_{\mathrm{f}})-(\hat{m}-1)\varphi_1(k_{\mathrm{f}}-k_1)}{(k_1+(\hat{m}-1)k_{\mathrm{f}})+\varphi_1(k_{\mathrm{f}}-k_1)}$
Electrical conduc.	$\frac{\sigma_{\mathrm{hnf}}}{\sigma_{\mathrm{bf}}} = \left(1+\frac{3\left(\frac{\sigma_2}{\sigma_{\mathrm{bf}}}-1\right)\varphi_2}{\left(\frac{\sigma_2}{\sigma_{\mathrm{bf}}}+2\right)-\left(\frac{\sigma_2}{\sigma_{\mathrm{bf}}}-1\right)\varphi_2}\right),$	$\frac{\sigma_{\mathrm{bf}}}{\sigma_{\mathrm{f}}} = \left(1+\frac{3\left(\frac{\sigma_1}{\sigma_{\mathrm{f}}}-1\right)\varphi_1}{\left(\frac{\sigma_1}{\sigma_{\mathrm{f}}}+2\right)-\left(\frac{\sigma_1}{\sigma_{\mathrm{f}}}-1\right)\varphi_1}\right)$

As a base fluid, blood was employed. Fe_3O_4 nanoparticles and carbon nanotubes (CNTs) were utilized in a ratio of 50/50, respectively. In two steps, samples were generated using carbon nanotubes and Fe_3O_4 nanoparticles. The thermophysical characteristics of blood and both types of $Fe_3O_4$and CNTs are shown in Table 2.

Table 2. Thermal properties of the base fluid (blood), Fe_3O_4, and CNTs [23-24].

Feature	$\boldsymbol{\rho}$ (kg/m ^{3})	$\boldsymbol{c_p}$(J/kg.K)	$\boldsymbol{k}$ (W/m.K)	$\boldsymbol{\beta x 10^5}(K^{-1})$
Human blood	1053	3594	0.492	0.18
SWCNTs	2600	425	6600	27
MWCNTs	1600	765	3000	44

The equations are converted into a dimensionless format by introducing the following non-dimensional parameters:

$$\left.\begin{aligned} \eta = \mathrm{y}\left(\frac{c}{\nu_f}\right)^{1/2}, u(\mathrm{u}_p)(\eta) = \mathrm{cx}F'(F_p')(\eta), v = -(c\nu_f)^{1/2}F(F_p')(\eta), \\ \mathrm{N} = \mathrm{cx}\left(\frac{c}{\nu_f}\right)^{1/2}\mathrm{H}(\eta),\ \theta(\theta_p)(\eta) = \frac{T(T_p)-T_\infty}{T_w-T_\infty}. \end{aligned}\right\} \quad (17)$$

Equations (8) and (12) are satisfied automatically and Eqs. (9) - (16) yield

$$\left(\frac{\mu_{hnf}}{\mu_f}+A\right)\mathrm{F}''' - \frac{\rho_{hnf}}{\rho_f}\left(\mathrm{F}'^2 - \mathrm{FF}'' - \frac{\beta_{hnf}}{\beta_f}\lambda\theta\right) + \mathrm{L}\beta_v(F_p' - \mathrm{F}') + \mathrm{AH}' - \frac{\mu_{hnf}}{\mu_f}\epsilon\mathrm{F}' + \chi e^{(-B\eta)} = 0 \quad (18)$$

$$\frac{(\rho c_p)_f}{(\rho c_p)_{hnf}}\left(\frac{K_{hnf}}{K_f}+R_d\right)\theta'' + \mathrm{Pr}\,[\mathrm{L}\beta_T(\theta_p-\theta) + \mathrm{L}\beta_v E_c(F_p'-\mathrm{F}')^2 - \delta(\mathrm{F}'^2\theta - FF''\theta - FF'\theta' + F^2\theta'') - \frac{(\rho c_p)_f}{(\rho c_p)_{hnf}}\mathrm{Q}(F'\theta - F\theta')) - F'\theta + F\theta'] + \frac{(\rho c_p)_f}{(\rho c_p)_{hnf}}\mathrm{Q}\theta = 0 \quad (19)$$

$$\frac{\rho_f}{\rho_{hnf}}\left(\left(\frac{\mu_{hnf}}{\mu_f}+\frac{A}{2}\right)H'' - \mathrm{AB}^*(2H+F'')\right) - F'H + FH' = 0 \quad (20)$$

$$\mathrm{F}_p F_p'' - F_p'^2 + \beta_v(\mathrm{F}' - F_p') = 0 \tag{21}$$

$$F_p'\theta_p - \mathrm{F}_p\theta_p' + \gamma\beta_T\left(\theta_p - \theta\right) = 0 \tag{22}$$

with

$$F(0) = 0, F'(0) = 1, \theta(0) = 1, H(0) = -\mathrm{n}F''(0) \tag{23}$$

$$F'(F_p')(\infty) \to 0,\ F_p\ (\infty) \to F(\infty),\ \theta(\theta_p)(\infty) \to 0,\ H(\infty) \to 0 \tag{24}$$

where,

$$\frac{\mu_{hnf}}{\mu_f} = D = \frac{1}{(1-\varphi_{CNTs})^{25/10}(1-\varphi_{FO})^{25/10}}.$$

$$\frac{\rho_{hnf}}{\rho_f} = D_1 = (1-\varphi_{FO})\left((1-\varphi_{CNTs}) + \varphi_{CNTs}\left(\frac{\rho_{CNTs}}{\rho_f}\right)\right) + \varphi_{FO}\left(\frac{\rho_{FO}}{\rho_f}\right).$$

$$\frac{(\rho\beta)_{hnf}}{(\rho\beta)_f} = D_2 = (1-\varphi_{FO})\left((1-\varphi_{CNTs}) + \varphi_{CNTs}\left(\frac{(\rho\beta)_{CNTs}}{(\rho\beta)_f}\right)\right) + \varphi_{FO}\left(\frac{(\rho\beta)_{FO}}{(\rho\beta)_f}\right).$$

$$\frac{(\rho c_p)_{hnf}}{(\rho c_p)_f} = D_3 = (1-\varphi_{FO})\left((1-\varphi_{CNTs}) + \varphi_{CNTs}\left(\frac{(\rho c_p)_{CNTs}}{(\rho c_p)_f}\right)\right) + \varphi_{FO}\left(\frac{(\rho c_p)_{FO}}{(\rho c_p)_f}\right).$$

$$\frac{K_{hnf}}{K_f} = D_4 = \frac{\left(K_{CNTs} + (\hat{m}-1)K_f\right) - (\hat{m}-1)\varphi_{CNTs}(K_f - K_{CNTs})}{\left(K_{CNTs} + (\hat{m}-1)K_f\right) + \varphi_{CNTs}(K_f - K_{CNTs})} \times$$

$$\frac{\left(K_{FO} + (\hat{m}-1)K_f\right) - (\hat{m}-1)\varphi_{FO}(K_f - K_{FO})}{\left(K_{FO} + (\hat{m}-1)K_f\right) + \varphi_{FO}(K_f - K_{FO})}.$$

The parameters and non-dimensional numbers are specified as

$\mathrm{Pr} = (\frac{\mu c_p}{k})_f$, $\lambda = \frac{Gr_x}{Re^2}$, $Gr_x = \frac{g\beta_f(T_w - T_\infty)x^3}{\nu_f^2}$, $Re = \frac{xu_w}{\nu_f}$, $\epsilon = \frac{\nu_f}{cK_p}$, $E_c = \frac{(cx)^2}{(c_p)_f\,(T_w - T_\infty)}$, $R_d = \frac{16\sigma^* {T_\infty}^3}{3k^{**}K_f}$, $Q = \frac{Q_0}{c(\rho c_p)_f}$, $\delta = \mathrm{c}\gamma_T$, $A = \frac{k}{\mu_f}$, $\chi = \frac{\pi j_0 M_0}{8c^2 x\rho_f}$, $\beta_v = \frac{1}{\mathrm{c}\tau_v}$, $\beta_T = \frac{1}{\mathrm{c}\tau_T}$, $\tau_v = \frac{m}{k^*}$, $m = \frac{\rho_p}{s}$, $\gamma = \frac{(c_p)_f}{c_m}$, $\mathrm{B} = \frac{\pi}{a}\sqrt{\frac{\nu_f}{c}}$, $\rho_\mathrm{p} = L\rho_\mathrm{f}$.

The significant physical quantities in engineering include the skin friction coefficient denoted as C_f and the local Nusselt number represented by N_u.These parameters are defined as:

$$C_f = \frac{\tau_w}{\rho_f u_\mathrm{w}^2},\quad N_u = \frac{xq_w}{k_f\,(T_w - T_\infty)} \tag{25}$$

where

$\tau_w = \mu_{hnf}\left(\partial_y u\right)_{y=0}$, $q_w = -k_{hnf}\left(\partial_y T\right)_{y=0} + q^r$.

The dimensionless form of Eq. (16) takes the form.

$$R_e^{1/2}C_f = \frac{\mu_{hnf}}{\mu_f}\mathrm{F}''(0), R_e^{-1/2}N_u = -(\frac{k_{hnf}}{k_f} + R_d)\theta'(0). \tag{26}$$

5. Methods

Non-linear governing ODEs (18)-(22) and corresponding boundary conditions (23)- (24) are solved using MATLAB bvp4c. We converted the nonlinear governing ODE into a set of 1^{ft}-order differential equations. The procedure involved considering the following factors:

$$\mathrm{F} = \widehat{\mathrm{Y}}_1, F' = \widehat{\mathrm{Y}_2}, \mathrm{F}'' = \widehat{\mathrm{Y}}_3, \theta = \widehat{\mathrm{Y}}_4, \theta' = \widehat{\mathrm{Y}}_5, \mathrm{H} = \widehat{\mathrm{Y}}_6, \mathrm{H}' = \widehat{\mathrm{Y}}_7, F_p = \widehat{\mathrm{Y}}_8, F_p' = \widehat{\mathrm{Y}}_9, \theta_p = \widehat{\mathrm{Y}}_{10}. \quad (27)$$

The first-order differential equations are as follows:

$$\mathrm{F}''' = \left[\frac{1}{\mathrm{D}+A}\right]\left(D_1\left(\widehat{\mathrm{Y}}_2^2 - \widehat{\mathrm{Y}}_1\widehat{\mathrm{Y}}_3 - D_2\lambda\widehat{\mathrm{Y}}_4\right) - \mathrm{L}\beta_v\left(\widehat{\mathrm{Y}}_9 - \widehat{\mathrm{Y}}_2\right) - \mathrm{A}\widehat{\mathrm{Y}}_7 + \mathrm{D}\epsilon\widehat{\mathrm{Y}}_2 - \chi e^{(-B\eta)}\right), \quad (28)$$

$$\theta'' = \left[\frac{1}{(1/D_3(D_4+R_d)-\mathrm{Pr}\delta\widehat{Y}_1^2)}\right]\left((-\mathrm{Pr})\left[\mathrm{L}\beta_T\left(\widehat{\mathrm{Y}}_{10} - \widehat{\mathrm{Y}}_4\right) + \mathrm{L}\beta_v E_c\left(\widehat{\mathrm{Y}}_9 - \widehat{\mathrm{Y}}_2\right)^2 - \delta\left(\widehat{Y}_2^2\widehat{\mathrm{Y}}_4 - \widehat{\mathrm{Y}}_1\widehat{\mathrm{Y}}_3\widehat{\mathrm{Y}}_4 - \widehat{\mathrm{Y}}_1\widehat{\mathrm{Y}}_2\widehat{\mathrm{Y}}_5\right) - \frac{1}{D_3}\mathrm{Q}\left(\widehat{\mathrm{Y}}_2\widehat{\mathrm{Y}}_4 - \widehat{\mathrm{Y}}_1\widehat{\mathrm{Y}}_5\right)\right) - \widehat{\mathrm{Y}}_2\widehat{\mathrm{Y}}_4 + \widehat{\mathrm{Y}}_1\widehat{\mathrm{Y}}_5\right] + \frac{1}{D_3}\mathrm{Q}\widehat{\mathrm{Y}}_4\right), \quad (29)$$

$$H'' = \left[\frac{1}{(1/D_1(\mathrm{D}+A/2))}\right]\left(\left(\frac{1}{D_1}\right)AB^*\left(2\widehat{\mathrm{Y}}_6 + \widehat{\mathrm{Y}}_3\right) + \widehat{\mathrm{Y}}_2\widehat{\mathrm{Y}}_6 - \widehat{\mathrm{Y}}_1\widehat{\mathrm{Y}}_7\right), \quad (30)$$

$$F_p'' = \frac{1}{\mathrm{Y}_8}\left(\widehat{Y}_9^2 + \beta_v(\widehat{\mathrm{Y}}_2 - \widehat{\mathrm{Y}}_9)\right), \quad (31)$$

$$\theta_p' = \frac{1}{\mathrm{Y}_8}\left(\widehat{\mathrm{Y}}_9\widehat{\mathrm{Y}}_{10} + \gamma\beta_T\left(\widehat{\mathrm{Y}}_{10} - \widehat{\mathrm{Y}}_4\right)\right). \quad (32)$$

The boundary conditions equations (23)-(24) are as follows:

$$\widehat{\mathrm{Y}}_1 = 0, \quad \widehat{\mathrm{Y}}_2 = 1, \quad \widehat{\mathrm{Y}}_4 = 1, \quad \widehat{\mathrm{Y}}_6 = n\widehat{\mathrm{Y}}_3 \qquad at\eta = 0 \quad (33)$$

$$\widehat{\mathrm{Y}}_2 = 0, \quad \widehat{\mathrm{Y}}_9 = 0, \quad \widehat{\mathrm{Y}}_8 = \widehat{\mathrm{Y}}_1, \quad \widehat{\mathrm{Y}}_4 = 0, \quad ,\widehat{\mathrm{Y}}_{10} = 0, \quad \widehat{\mathrm{Y}}_6 = 0 \qquad as\ \eta \longrightarrow \infty \quad (34)$$

The Matlab bvp4c solver employs these first-order differential equations and boundary conditions to investigate the impact of variables on consecutive profiles.

6. Results and Discussion

A mathematical exploration has been exhibited to examine the impacts of the dust micropolar hybrid flow of hybrid nanofluids over a Riga surface subjected to the influence of C-C with heat generation impact. The consequences of several considerable system parameters on the flow pattern have been thoroughly debated in the previous section. Some important observations are summarized below:

Table 3: The specific numerical values of local Nusselt Number for various values of Pr when $A = \lambda = L = \beta_v = \varepsilon = \chi = B = R_d = \beta_T = Ec = \delta = Q = B_1 = n = \gamma = 0$.

Pr	**Mahdy [47]**	**Das et al.[48]**	**Present Study**
0.72	0.80868	0.80876	0.80863
1.00	1.00000	1.00000	1.00000
3.00	1.92368	1.92357	1.92368
7.00	3.07224	3.07314	3.07225
10.0	3.72067	3.72055	3.72067

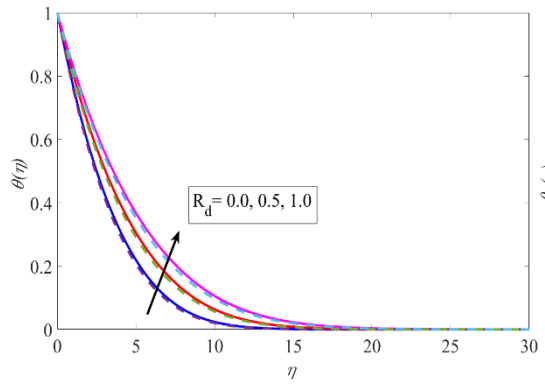

——— (SWCNT-Fe_3O_4)

--------- (MWCNT-Fe_3O_4)

Figure-3: Impact of R_d $\theta(\eta)$

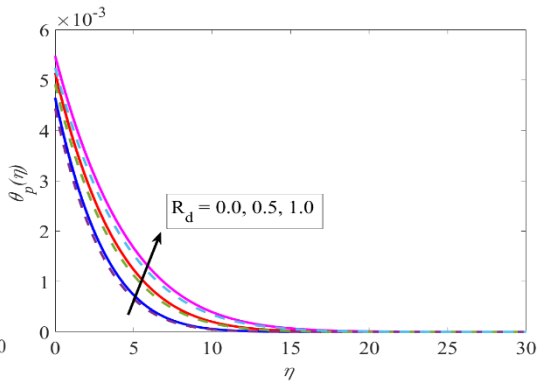

——— (SWCNT-Fe_3O_4)

--------- (MWCNT-Fe_3O_4)

Figure-4: Impact of $R_d$on $\theta_p(\eta)$

when $A = \lambda = L = \beta_v = \varepsilon = \chi = B = \eta = R_d = \beta_T = Ec = \delta = Q = B_1 = n = \gamma = 0.1$.

Figure 3-4: Depict the influence of R_d on temperature profiles (θ) for SWCNT-Fe3O4 and MWCNT-Fe3O4 nanofluids. Increasing R_d leads to notable changes in temperature distribution along the Riga surface (η), indicating alterations in heat transfer characteristics. These changes are attributed to enhanced thermal radiation effects, impacting heat transfer rates near the surface.

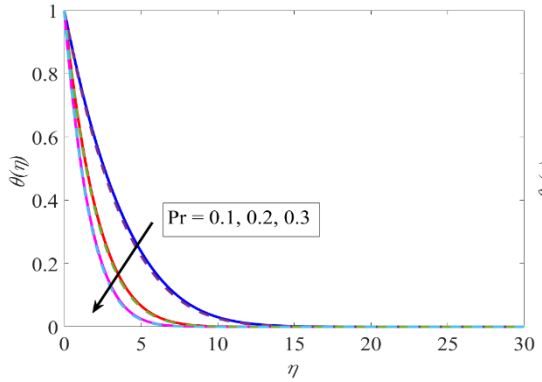

——— (SWCNT-Fe_3O_4)

--------- (MWCNT-Fe_3O_4)

Figure-5: Impact of Pr $\theta(\eta)$

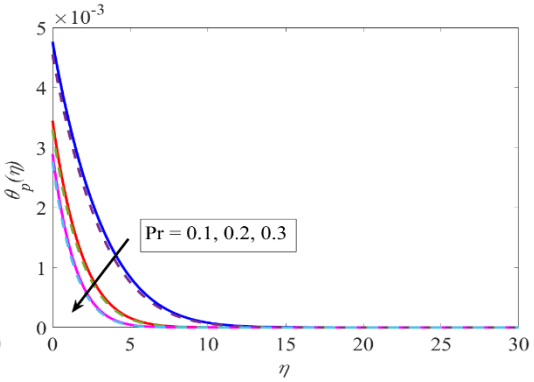

——— (SWCNT-Fe_3O_4)

--------- (MWCNT-Fe_3O_4)

Figure-6: Impact of Pr on $\theta_p(\eta)$

when $A = \lambda = L = \beta_v = \varepsilon = \chi = B = R_d = \beta_T = Ec = \delta = Q = B_1 = n = \gamma = 0.1.$

These figures demonstrate how the Prandtl number (Pr) influences temperature profiles (θ_p) for different nanofluid compositions. They show how changing Pr affects the distribution of temperature within the nanofluid, providing insights into the thermal behavior of the system.

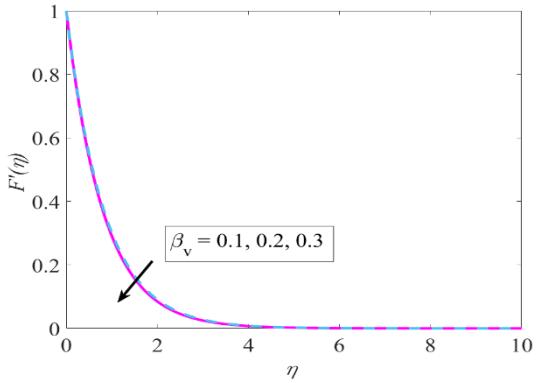

———(SWCNT-Fe_3O_4)

--------- (MWCNT-Fe_3O_4)

Figure-7: Impact of β_v on $F'(\eta)$

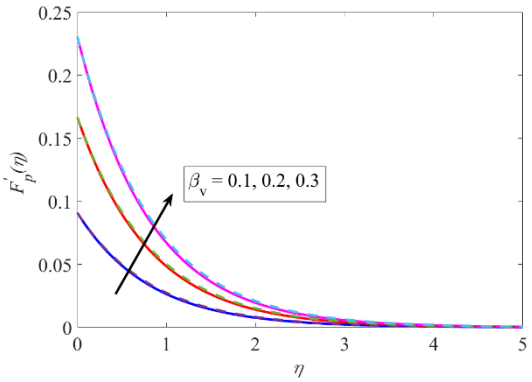

———(SWCNT-Fe_3O_4)

--------- (MWCNT-Fe_3O_4)

Figure-8: Impact of β_v on $F_p'(\eta)$

when $A = \lambda = L = \beta_v = \varepsilon = \chi = B = R_d = \beta_T = Ec = \delta = Q = B_1 = n = \gamma = 0.1$

Figure 7-8: Here, the effect of the fluid-particle interaction parameter β_v on velocity profiles (F and F_p') is depicted. These figures explore how variations in β_v impact the flow velocity in both the fluid and particle phases, indicating changes in the flow characteristics.

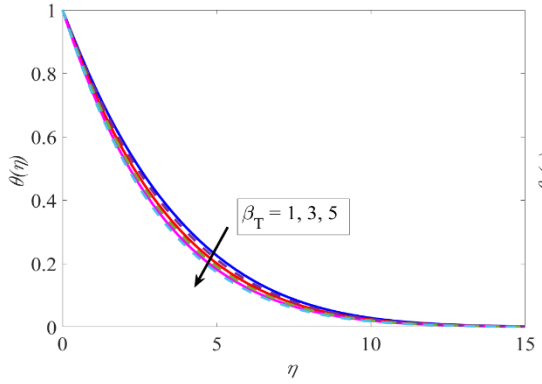

——— (SWCNT-Fe_3O_4)

-------- (MWCNT-Fe_3O_4)

Figure-9: Impact of β_T on $\theta(\eta)$

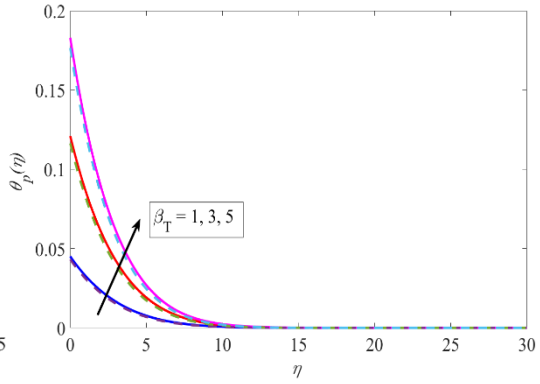

——— (SWCNT-Fe_3O_4)

--------- (MWCNT-Fe_3O_4)

Figure-10: Impact of β_T on $\theta_p(\eta)$

when $A = \lambda = L = \beta_v = \varepsilon = \chi = B = R_d = \beta_T = Ec = \delta = Q = B_1 = n = \gamma = 0.1$

Figure 9-10: These figures illustrate the influence of the fluid particle interaction parameter for temperature (β_T) on temperature profiles (θ and θ_p) for different nanofluid compositions. They show how altering βT affects the temperature distribution within the nanofluid, providing insights into the heat transfer behavior of the system.

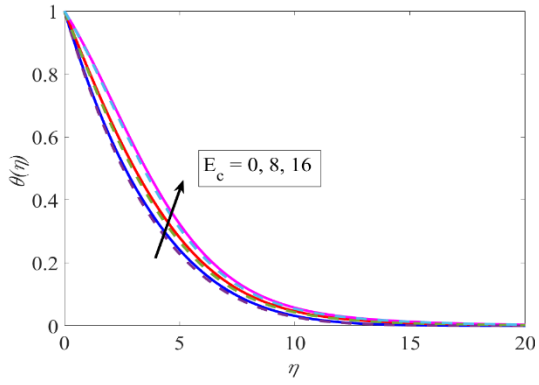

——(SWCNT-Fe_3O_4)

--------- (MWCNT-Fe_3O_4)

Figure-11: Impact of Ec on $\theta(\eta)$

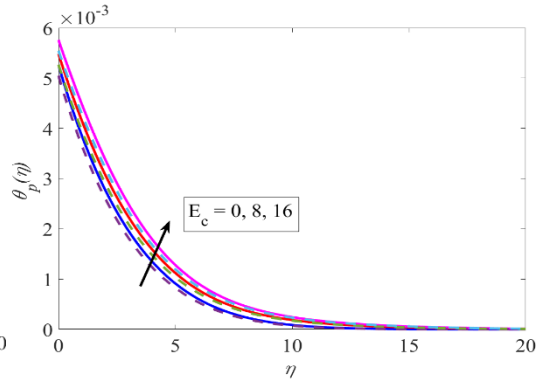

——— SWCNT-Fe_3O_4)

--------- (MWCNT-Fe_3O_4)

Figure-12: Impact of Ec on $\theta_p(\eta)$

when $A = \lambda = L = \beta_v = \varepsilon = \chi = B = \eta = R_d = \beta_T = Ec = \delta = Q = B_1 = n = \gamma = 0.1$

Figure 11-12: The impact of Eckert number (Ec) on temperature profiles (θ and θp) for various nanofluid compositions is demonstrated here. These figures highlight how changing Ec influences the temperature distribution within the nanofluid, indicating alterations in the heat transfer characteristics.

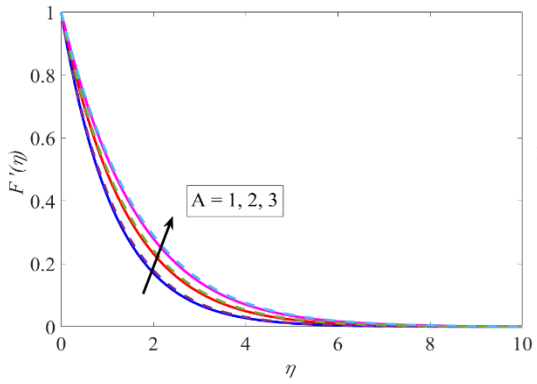

——— (SWCNT-Fe_3O_4)

---------(MWCNT-Fe_3O_4)

Figure-13: Impact of A on $F'(\eta)$

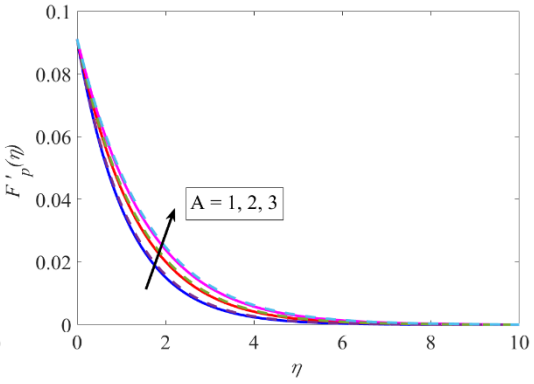

———(SWCNT-Fe_3O_4)

--------- (MWCNT-Fe_3O_4)

Figure-14: Impact of A on $F_p'(\eta)$

when $A = \lambda = L = \beta_v = \varepsilon = \chi = B = R_d = \beta_T = Ec = \delta = Q = B_1 = n = \gamma = 0.$

Figure 13-14: Here, the effect of the micropolar parameter (A) on velocity profiles (F′ and F_p') for different nanofluid compositions is illustrated. These figures explore how variations in A impact the flow velocity in both the fluid and particle phases, indicating changes in the flow behavior.

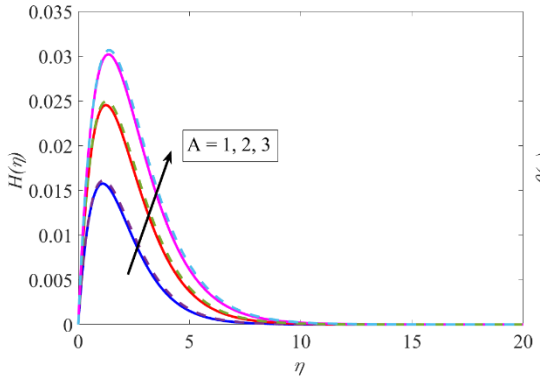

———(SWCNT-Fe_3O_4)

--------- (MWCNT-Fe_3O_4)

Figure-15: Impact of A on H (η), when

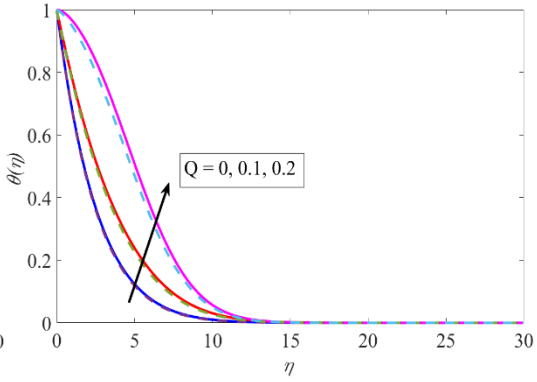

———(SWCNT-Fe_3O_4)

--------- (MWCNT-Fe_3O_4)

Figure-16: Impact of Q on $\theta(\eta)$

when

$B^* = \beta_v = 0.1, \varepsilon = \chi = B = \eta = R_d$ $A = \lambda = \beta_T = Ec = \delta = Q = Pr = n = \gamma = 0.$

$A = \lambda = L = B^* = \beta_v =, \varepsilon = \chi = B = \beta_T = Ec = \delta = Q = Pr = n = \gamma = 0.1.$

Figure 15-16: These figures show the impact of heat generation parameter (Q) on temperature profiles (θ and θ_p) for different conditions. They demonstrate how altering Q affects the temperature distribution within the system, providing insights into the heat generation effects.

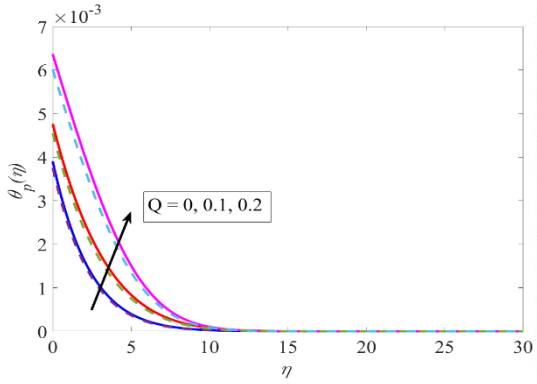

(SWCNT-Fe_3O_4)

--------- (MWCNT-Fe_3O_4)

Figure-17 Impact of Q on $\theta_p(\eta)$

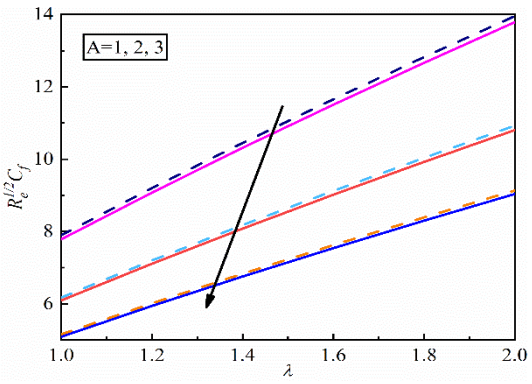

(SWCNT-Fe_3O_4)

--------- (MWCNT-Fe_3O_4)

Figure-18: Impact of A and λ on C_f.

when $A = \lambda = L = \beta_v = \varepsilon = \chi = B^* = \eta = R_d = L = \beta_v = \varepsilon = \chi = B^* = \eta = R_d = \beta_T = Ec = \delta = Q = Pr = n = B = \gamma = 0.1$. $\beta_T = Ec = \delta = Q = Pr = n = B = \gamma = 0.1$.

Figure 17-18: The influence of parameters A and λ on skin friction coefficient (C_f) for different conditions is depicted in these figures. They explore how changes in A and λ affect the frictional forces experienced by the fluid, providing insights into the flow behavior over the surface.

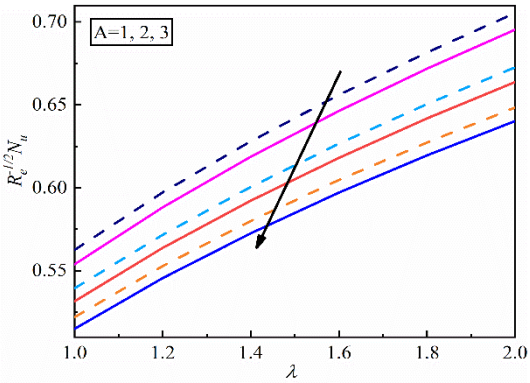

(SWCNT-Fe_3O_4)

--------- (MWCNT-Fe_3O_4)

Figure-19: Impact of A and λ on N_u,

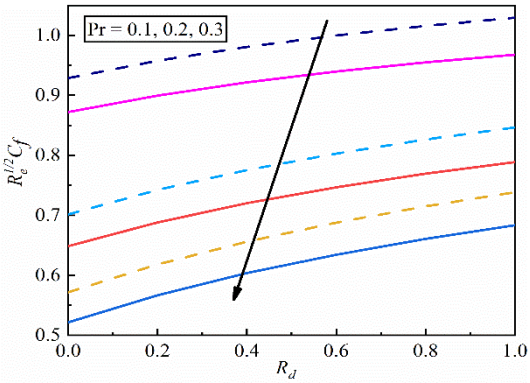

(SWCNT-Fe_3O_4)

--------- (MWCNT-Fe_3O_4)

Figure-20: Impact of Pr and R_d on C_f,

When $L = \beta_v = \varepsilon = \chi = B^* = \eta = R_d = B^*$ = when $A = L = \beta_v = \varepsilon = \chi = \beta_T = Ec = \delta = Q = Pr = n = B = \gamma = 0.1$. $\beta_T = Ec = \delta = Q = \lambda = n = B = \gamma = 0.1$.

Figure 19-20: Here, the effect of Prandtl number (Pr) and non-linear thermal radiation parameter (R_d) on skin friction coefficient (C_f) for different conditions is illustrated. These

figures explore how variations in Pr and R_d impact the frictional forces experienced by the fluid, providing insights into the heat transfer characteristics.

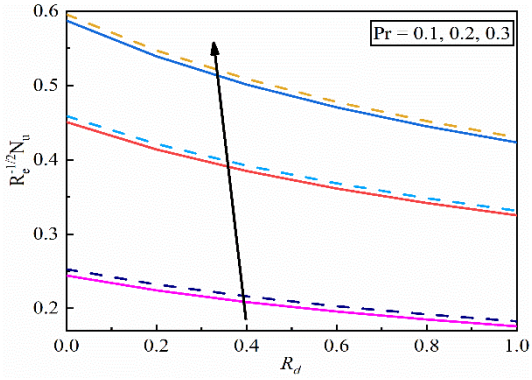

——— (SWCNT-Fe_3O_4)

--------- (MWCNT-Fe_3O_4)

Figure 21: Impact of Pr and R_d on Nu when $A = \lambda = L = \beta_v = \varepsilon = \chi = B = \eta = B^* = \beta_T = Ec = \delta = Q = n = \gamma = 0.1$

Figure 21: This figure demonstrates the impact of Prandtl number (Pr) and non-linear thermal radiation parameter (R_d) on the local Nusselt number (Nu) for specified conditions. It explores how variations in Pr and R_d influence the convective heat transfer rate at the surface, providing insights into the heat transfer behavior of the system.

Overall, these figures offer comprehensive insights into the influence of various parameters on the thermal and flow characteristics of micropolar hybrid nanofluid flows over a Riga surface, aiding in the understanding and optimization of such systems in engineering applications.

7. Conclusion

In summary, this study comprehensively investigates the dynamics of nanofluid flows over a Riga surface, considering parameters like R_d, Pr, and βv. The findings highlight their significant impact on temperature distribution, fluid flow patterns, and friction forces. The results offer insights crucial for optimizing engineering systems like cooling technologies and heat exchangers. This research advances our understanding of nanofluid dynamics and provides valuable guidance for future studies and practical applications.

Refrences

[1] J. Radushkevich, B. Lukyanovich,. О Структуре Углерода, Образующегося При Термическом Разложении Окиси Углерода На Железном Контакте (1952).
[2] Iijima S., Helical microtubules of graphitic carbon, Nature 354, (1991). 56–58 17.
[3] Murshd SMS, Leong KC, Yang C. Enhanced thermal conductivity of TiO2- Water based nanofluid. Int J Ther Sci. (2005) 4:367–73. doi: 10.1016/j.ijthermalsci.2004.12.005.
[4] Baughman R., Zakhidov A., Heer W. Carbon nanotubes- the route toward applications. Science. (2002) 297:787–92. doi: 10.1126/science.1060928.

[5] Ericson LM, Fan H, Peng H, Davis VA, Zhou W. Macroscopic neat single-walled carbon nanotube fibers. Science. (2004) 305:1447–50. doi: 10.1126/science.1101398.
[6] Milne I., Teo K., Amaratunga G., Legagneux P., Gangloff L., Schnell P. ,Carbon nanotubes as field emission sources, J Mat Chem. (2004) 14:933–43. doi: 10.1039/b314155c
[7] Choi, S., Lockwood, F. , Grulke, E., Zhang, Z., Yu, W., Anomalous thermal conductivity enhancement in nanotube suspensions, Appl. Phys. Lett. 2001, 79, 2252–2254.
[8] Duong H., Papavassiliou D., Mullen K., Wardle B., Maruyama Sh. ,Calculated Thermal Properties of Single-Walled Carbon Nanotube Suspensions , J. Phys. Chem. C 2008, 112, 19860–19865.
[9] Rashmi W., Ismail A. , Sopyan I. , Jameel A., Yusof F. , Khalid M. , Mubarak N., Stability and thermal conductivity enhancement of carbon nanotube nanofluid using gum arabic , J. of Exp. Nano. 2011, https://doi.org/10.1080/17458080.2010.487229.
[10] T. Hayat,1 M. Farooq,1 and A. Alsaedi, Homogeneous-heterogeneous reactions in the stagnation point flow of carbon nanotubes with Newtonian heating , AIP ADVANCES, (2015), https://doi.org/10.1063/1.4908602.
[11] Estellé P., Halelfadl S. ,Thermal conductivity of CNT water based nanofluids: experimental trends and models overview , J. of Ther. Engi. (2015) 1, 2, 381-390.
[12] Iqbal Z., Azhar E. , Maraj E., Transport phenomena of carbon nanotubes and bioconvection nanoparticles on stagnation point flow in presence of induced magnetic field , Physica E 91 (2017) 128–135 http://dx.doi.org/10.1016/j.physe.2017.04.022.
[13] Nasir S., Shah Z., Islam S., Bonyah E., Gul T., Darcy Forchheimer nanofluid thin film flow of SWCNTs and heat transfer analysis over an unsteady stretching sheet, AIP Advances (2019), 9, doi: 10.1063/1.5083972.
[14] Rahman J., Khan U., Ahmad Sh., Ramzan M., Suleman M., Lu D., Inam S., Numerical Simulation of Darcy-Forchheimer 3D Unsteady Nanofluid Flow Comprising Carbon Nanotubes with Cattaneo-Christov Heat Flux and Velocity and Thermal Slip Conditions, Processes (2019), 7, 687; doi:10.3390/pr7100687.
[15] Hayat T. , Khan S. , A. Alsaedi, Zia Q. ,Irreversibility analysis in Darcy-Forchheimer flow of CNTs with dissipation and Joule heating effects by a curved stretching sheet, Applied Nanoscience 11 (2021) 187–198 https://doi.org/10.1007/s13204-020-01566-w
[16] Reddy P., Sreedevi P., Reddy V. , Entropy generation and heat transfer analysis of magnetic nanofluid flow inside a square cavity filled with carbon nanotubes, Chem. Therm. and Ther. Anal. 6 (2022) 100045 https://doi.org/10.1016/j.ctta.2022.100045.
[17] Manaa N., Abidi A., Estellé P., Borjini M., Numerical simulation of three-dimensional thermo-solutal convection of micropolar multi-walled carbon nanotubes water nanofluid stabilized by lignin and sodium polycarboxylate, J. of Ther. Anal. and Calo. 147 (2022) 2985–3005 https://doi.org/10.1007/s10973-021-10667-9.
[18] S. Mehryan, M. Izadi, Z. Namazian, A. Chamkha ,Natural convection of multi-walled carbon nanotube–Fe3O4/water magnetic hybrid nanofluid flowing in porous medium considering the impacts of magnetic field-dependent viscosity, J. of Ther. Anal. and Calo. 138 (2019) 1541–1555 https://doi.org/10.1007/s10973-019-08164-1.
[19] Liu Ch., Duan Y., Cai J., Li X., Zhang D., Gao J. , Che Y. Compressible Fe3O4/MWCNTs-coated polymer foams for high-performance and tunable electromagnetic microwave absorption, Materials Research Express, 6 (10) (2019) 106114.
[20] Tassaddiq A., Khan S., Bilal M., Gul T., Mukhtar S., Shah Z., et al. ,Heat and mass transfer together with hybrid nanofluid flow over a rotating disk, AIP Adv. 10 (5) (2020) 055317.
[21] Shah Z. , Saeed A., Khan I. , Selim M., Ikramullah , Kumam P. ,Numerical modeling on hybrid nanofluid (Fe3O4+MWCNT/H2O) migration considering MHD effect over a porous cylinder , PLOS ONE (2021) https://doi.org/10.1371/journal.pone.0251744.
[22] Saeed A. , Alghamdi W., Mukhtar S., Shah S. , Kumam P., Gul T. , Nasir S. , Kumam W., Darcy-Forchheimer hybrid nanofluid flow over a stretching curved surface with heat and mass transfer, PLOS ONE (2021) https://doi.org/10.1371/journal.pone.0249434.

[23] Khan M., Mei S., Shabnam , Fernandez- Gamiz U., Noeiaghdam S., Shah S. , Khan A., Numerical Analysis of Unsteady Hybrid Nanofluid Flow Comprising CNTs-Ferrousoxide/Water with Variable Magnetic Field, Nanomaterials 12 180 (2022) https://doi.org/10.3390/nano12020180.
[24] Khan M., Mei S., Shabnam , Shah N., Chung J., Khan A., Shah S., Steady Squeezing Flow of Magnetohydrodynamics Hybrid Nanofluid Flow Comprising Carbon Nanotube-Ferrous Oxide/Water with Suction/Injection Effect, Nanomaterials 2022, 12, 660. https://doi.org/10.3390/nano12040660.
[25] M. Krishnamurthy ,MHD Flow And Radiative Heat Transfer Of Micropolar Dusty Fluid Suspended With Alumina Nanoparticles Over A Stretching Sheet Embedded In A Porous Medium, JNNCE Journal of Engineering & Management (JJEM) 2 (1) (2018).
[26] Eid M. , Mabood F. , Entropy analysis of a hydromagnetic micropolar dusty carbon NTs-kerosene nanofluid with heat generation: Darcy–Forchheimer scheme ,J of Ther Anal and Calo (2021) 143:2419–2436 https://doi.org/10.1007/s10973-020-09928.
[27] Nabwey H. , Mahdy A., Transient flow of micropolar dusty hybrid nanofluid loaded with Fe3O4-Ag nanoparticles through a porous stretching sheet, Results in Physics 21 (2021) 103777 https://doi.org/10.1016/j.rinp.2020.103777.
[28] Kaneez H., Alebraheem J., Elmoasry A., Saif R. , Nawaz M., Numerical investigation on transport of momenta and energy in micropolar fluid suspended with dusty, mono and hybrid nano-structures, AIP Advances 10, 045120 (2020); doi: 10.1063/5.0003042.
[29] Fourier JBJ, TheAˆ orie Analytique De La Chaleur. Paris 1822. 28.
[30] Cattaneo C. Sulla conduzione del calore. Atti Semin Mat Fis Univ Modena Reggio Emilia. 3 (1948) 83-101.
[31] Christov CI. On frame indifferent formulation of the Maxwell-Cattaneo model of finite-speed heat conduction. Mech Res Commun. 36 (2009) 481–486. https://doi.org/10.1016/j.mechrescom.2008.11.003.
[32] Tassaddiq A., Impact of Cattaneo-Christov heat flux model on MHD hybrid nano-micropolar fluid flow and heat transfer with viscous and joule dissipation effects, Scien. Repo. (2021) 11:67 https://doi.org/10.1038/s41598-020-77419-x.
[33] Siddiq M., Ashraf M. ,Bioconvection of micropolar nanofluid with modified Cattaneo–Christov theories , Adva. in Mech. Engin. 12(5) (2020), 1–11 DOI: 10.1177/1687814020925217.
[34] Ramzan M., Gul H. , Baleanu D., K. Nisar , M. Malik ,Role of Cattaneo–Christov heat flux in an MHD Micropolar dusty nanofluid flow with zero mass flux condition, Scie. Repo. (2021) 11:19528 https://doi.org/10.1038/s41598-021-98988-5.
[35] Shankaralingappa B. , Gireesha B. , Prasannakumara B. , Nagaraja B. , Darcy-Forchheimer flow of dusty tangent hyperbolic fluid over a stretching sheet with Cattaneo-Christov heat flux, Wav. in Rand. and Comp. Med.2021 https://doi.org/10.1080/17455030.2021.1889711.
[36] Upadhay M.S. , Raju M.C., Cattaneo-Christov on heat and mass transfer of unsteady Eyring Powell dusty nanofluid over sheet with heat and mass flux conditions, Infor. in Medic. Unlo. 9 (2017) 76 - 85http://creativecommons.org/licenses/by-nc-nd/4.0/).
[37] Gailitis A. ,On the possibility to reduce the hydrodynamic drag of a plate in an electrolyte, Appl. Magnetohydrodyn. Rep. Inst. Phys. Riga 1961, 13, 143–146.
[38] Ali B. , Devi S., Hussein A. , Hussain S., Naqvi R., Transient rotating nanofluid flow over a Riga plate with gyrotactic micro-organisms, binary chemical reaction and non-Fourier heat flux, Chin. J. of Phys. 73 (2021) 732–745 https://doi.org/10.1016/j.cjph.2021.07.031.
[39] Anjum A., Mir N. , Farooq M. , Javed M. , Ahmad S. , Malik M. , Alshomrani A., Physical aspects of heat generation/absorption in the second grade fluid flow due to Riga plate: Application of Cattaneo-Christov approach, Resu. in phys. 9(2018) 955-960 https://doi.org/10.1016/j.rinp.2018.03.024.
[40] Alotaibi H. , Rafique Kh., Numerical Analysis of Micro-Rotation Effect on Nanofluid Flow for Vertical Riga Plate , Cryst.(2021), 11, 1315. https://doi.org/10.3390/cryst11111315.
[41] Abbas N. , Nadeem S., Malik M., Theoretical study of micropolar hybrid nanofluid over Riga channel with slip conditions, Phys. A 551 (2020) 124083 https://doi.org/10.1016/j.physa.2019.124083.
[42] Nadeem S. , Amin A. , Abbas N. , Saleem A., Alharbi F. , Hussain A. , Issakhov A., Stagnation Point Flow of Micropolar Maxwell Fluid over Riga Plate under the Influence of Heat and Mass Transfer.

[43] Islam Md., Nasrin S., Micropolar Fluid Flow Along with an Inclined Riga Plate Through a Porous Medium , Inter. J. of Heat and Tech. 39 (4)(2021) 1123-1133.
[44] Alshehri A., Coban H., Ahmad Sh. , Khan U., Alghamdi W. ,Buoyancy Effect on a Micropolar Fluid Flow Past a Vertical Riga Surface Comprising Water-Based SWCNT–MWCNT Hybrid Nanofluid Subject to Partially Slipped and Thermal Stratification: Cattaneo–Christov Model , Math. Prob. in Engin. Volu.(2021) https://doi.org/10.1155/2021/6618395.
[45] Ahmed N. , Saba F. , Khan U. , Khan I., Alkanhal T. , Faisal I., Mohyud-Din S., Spherical Shaped (Ag − Fe3O4/H2O) Hybrid Nanofluid Flow Squeezed between Two Riga Plates with Nonlinear Thermal Radiation and Chemical Reaction Effects, Energies 2019, 12, 76; doi:10.3390/en12010076.
[46] Li Y., Shahb F., Khanc M., Chinramd R., Elmasrye Y., Sun T. ,Dynamics of Cattaneo-Christov Double Diffusion (CCDD) and arrhenius activation law on mixed convective flow towards a stretched Riga device, Chaos, Solitons and Fractals 148 (2021) 111010 https://doi.org/10.1016/j.chaos.2021.111010.
[47] A. Mahdy, Unsteady mixed convection boundary layer flow and heat transfer of nanofluids due to stretching sheet, Nucl. Eng. Des., 2012, 249, 248-255.
[48] S. Das, S. Chakraborty, R. N. Jana and O. D. Makinde, Entropy analysis of unsteady magneto-nanofluid flow past accelerating stretching sheet with convective boundary condition, Appl. Math. Mech. -Engl. Ed., 2015, 36(12), 1593-1610.